Journal of Magnetic Resonance 276 (2017) 69–77

Contents lists available at ScienceDirect

Journal of Magnetic Resonance

journal homepage: www.elsevier.com/locate/jmr

Longitudinal gradient coils with enhanced radial uniformity in restricted diameter: Single-current and multiple-current approaches

Javier A. Romero, Gabriela A. Domínguez, Esteban Anoardo *

Laboratorio de Relaxometría y Técnicas Especiales (LaRTE), Grupo de Resonancia Magnética Nuclear, FaMAF - Universidad Nacional de Córdoba e IFEG-CONICET, Córdoba, Argentina

ARTICLE INFO

Article history:
Received 31 August 2016
Revised 18 January 2017
Accepted 19 January 2017
Available online 21 January 2017

Keywords:
Gradient coils
Field-cycling
Multiple-current

ABSTRACT

An important requirement for a gradient coil is that the uniformity of the generated magnetic field gradient should be maximal within the active volume of the coil. For a cylindrical geometry, the radial uniformity of the gradient turns critic, particularly in cases where the gradient-unit has to be designed to fit into the inner bore of a compact magnet of reduced dimensions, like those typically used in fast-field-cycling NMR. In this paper we present two practical solutions aimed to fulfill this requirement. We propose a matrix-inversion optimization algorithm based on the Biot-Savart law, that using a proper cost function, allows maximizing the uniformity of the gradient and power efficiency. The used methodology and the simulation code were validated in a single-current design, by comparing the computer simulated field map with the experimental data measured in a real prototype. After comparing the obtained results with the target field approach, a multiple-element coil driven by independent current sources is discussed, and a real prototype evaluated. Opposed equispaced independent windings are connected in pairs conforming an arrangement of independent anti-Helmholtz units. This last coil seizes 80% of its radial dimension with a gradient uniformity better than 5%. The design also provides an adaptable region of uniformity along with adjustable coil efficiency.

1. Introduction

Magnetic field gradient coils as designed for magnetic resonance imaging (MRI) have several common aspects related to electromagnets for fast-field-cycling (FFC) nuclear magnetic resonance (NMR). In both cases we refer to coil devices that should be optimized for switched magnetic fields, with an optimized spatial uniformity of the generated field across a targeted volume of interest (VOI). In the case of gradient coils, the uniformity of the gradient is required [1,2], while in FFC magnets we refer to the magnetic field homogeneity [3–6]. In this manuscript we propose a robust and straightforward method for the design of longitudinal gradient coils based on a matrix inversion algorithm, successfully used also for the optimization of FFC magnets. The proposed solutions are validated in prototypes of simple construction.

For a given VOI, MRI machines are designed as compact as possible, since this has a direct impact in power consumption, which in turn leads to lower demands of power supply and cooling systems. In FFC machines one has to face, in addition, the fact that most of the variables affecting the performance of the system are related to the magnet volume. Most performance requirements for a gradient coil can be attended post fabrication. In fact, switching time can be handled with proper power amplifiers and power dissipation with efficient cooling. However, active corrections of the gradient uniformity inside the VOI demands for additional and complex hardware. For the reasons stated above, the present study focuses on producing longitudinal gradient coil designs with maximal exploitation of their active volume.

Three important aspects should be considered when designing a gradient coil for MRI:

(1) Maximize the gradient uniformity within the VOI. Spatial gradient homogeneity has a direct impact in image quality. A 5% deviation in uniformity represents a 5% error in pixel size in the final reconstructed image. This condition strictly depends on the geometry of the coil and its immunity to thermo-mechanical deformations.
(2) Facilitate rapid intensity variations of the gradient field. The switching performance, however, not only depends on the electrical parameters of the coil (inductance and resistance), but also on the powering network and the peripheral electronics.

* Corresponding author at: Famaf - UNC/IFEG – Conicet, Ciudad Universitaria, Córdoba, Argentina.
E-mail address: anoardo@famaf.unc.edu.ar (E. Anoardo).

http://dx.doi.org/10.1016/j.jmr.2017.01.012
1090-7807/

(3) Reach high gradient amplitudes without overheating (power dissipation). In practice, this last point mainly depends on the geometry and the net resistance of the winding, although an efficient cooling strategy may critically improve the performance.

There are different possibilities for the mathematical optimization of a gradient coil. In general, the problem is that of finding a current density pattern which fulfills the desired requirements. These requirements are then translated into a convenient set of equations, and then solved for the current density which best satisfies them. One of the most used methods is the target field approach [7], where the magnetic field is expressed in terms of a Fourier series expansion. This method was later expanded to include inductance as a variable to be minimized [8]. Finite elements methods include matrix inversion, like methods using the least-squares-error technique as applied to surface elements [9] and simulated annealing [10]. A matrix inversion of the Biot-Savart law combined with a Lagrange minimization of the dissipated power (subject to constraints on the homogeneity and effective volume) was successfully used to calculate FFC magnets [11]. A similar method including inductance minimization was proposed for optimizing gradient and radio frequency coils [12]. Stream function methods can also be applied to solve for the current density [13–15]. Other approaches take hot-spots into account [16], eddy currents [17], torque [18] and even the noise generated from switching [19].

The gradient coils here presented were designed for a FFC apparatus working with a cylindrical sample of 30 mm in diameter and 50 mm in length. The whole gradient coil unit is placed inside the bore of the main magnet [20]. Transversal gradient coils were adapted from other designs available in the literature [13,14]. However, we faced the problem of finding a longitudinal gradient coil design that will perform to our demands: generate a gradient field across the VOI with a maximum error of 5% in uniformity, with a coil diameter of 50 mm (inner gradient coil of the gradient unit). The restriction on the diameter of the coil comes from the dimensions of the main magnet: it implies the gradient coil must seize at least 60% of its radial dimension. Not being able to find a convenient design adaptable to our needs, we turned to the search for a simple and robust optimization method. Most designs of straightforward construction seize up to 50% of its radial dimension. Nevertheless non-tested mathematically elegant and fairly impracticable (or demanding absurd powering conditions) designs can be found in the literature claiming for a better performance. In turn, convenient as they are, many of the methods can represent a time-consuming challenge if not familiarized with the mathematical formulation or the numerical approach. A finite element method can become a cumbersome task and very imprecise to the non-expert, even using commercial solutions. The target field approach requires some advanced Fourier analysis skills. The stream function methods exhibit a prudent level of sophistication but the gradient uniformity tends to be poor:±5% within a volume of 40% of the coil radius [21].

We propose a simple "single-current" optimization algorithm which is based on the Biot-Savart law [9]. It solves for the optimal current density by means of a cost function. We place N equidistant conductors beforehand and solve for the driving current each conductor must have, instead of partitioning the cylindrical coil former in discrete elementary areas. The surface current density can then be approximated by a sufficiently large number of conductors. It corresponds to a matrix inversion algorithm, but the numerical approach is straightforward and convenient on computation time. The method also takes power dissipation into account to produce efficient (gradient/current) solutions [22].

The discrete solution for the optimal current density allowed us to investigate the performance of coils having a reduced number of localized and independent windings (multiple-current approach). We found that few elements can perform very well. Such is the case of the multiple-element coil we present in this work. With as few as 18 elements (equispaced, connected in pairs), it produces a magnetic field gradient that is uniform up to a ±2.5% error within a radius that encompasses 80% of its maximum value. The drawback is that it has to be driven by 9 independent current sources. There are a few papers and patents dealing with similar designs [23–25]. In our case, a set of combined anti-Helmholtz pair units are driven independently, thus saving half of the power supplies.

2. Optimization algorithm

Consider N coaxial, equispaced loop conductors along the Z-component of a cylindrical surface. The current of each ring is independent from each other. The magnetic field generated by this coil is calculated using the Biot-Savart law [26]:

$$B_Z\left(\vec{r}_k\right) = \sum_{n=1}^{N} c_n\left(\vec{r}_k\right) I_n$$

$$c_n\left(\vec{r}_k\right) = \frac{\mu_0}{4\pi} \int \frac{\vec{dl} \times \vec{r}}{r_k^2} \tag{1}$$

where I_n is the current of the n conductor and the integral in (1) is taken over all the spatial positions $\vec{r}_k$ within the VOI. Since we deal with non-pitched ideal rings, transversal magnetic components are negligible and completely irrelevant for the calculation. Therefore, only the Z-component of the magnetic field is considered. The magnetic field linearity and power dissipation requirements are now contemplated by means of a cost function [27]:

$$\Phi = \frac{1}{2}\sum_{k=1}^{K} \omega\left(\vec{r}_k\right)\left[B_Z\left(\vec{r}_k\right) - B_Z^t\left(\vec{r}_k\right)\right]^2 + \frac{\alpha}{2}\sum_{n=1}^{N} R_n I_n^2. \tag{2}$$

Here, $\omega\left(\vec{r}_k\right)$ and α are weighting factors. $\omega\left(\vec{r}_k\right)$ is a Gaussian-shaped function that focuses gradient uniformity at the center of the VOI, while α is a scalar for the account of the coil-efficiency. $B_Z^t\left(\vec{r}_k\right)$ is the predefined target region in space where the magnetic field must scale lineally with the Z coordinate. The optimal currents are found by minimizing the functional Φ:

$$0 = \frac{\partial \Phi}{\partial I_m} = \sum_{k=1}^{K} \omega\left(\vec{r}_k\right) c_m\left(\vec{r}_k\right)\left[\sum_{n=1}^{N} c_n\left(\vec{r}_k\right) I_n - B_Z^t\left(\vec{r}_k\right)\right] + \alpha R_n I_m.$$

These equations can be conveniently assembled into a global matrix equation

$$(\boldsymbol{G} + \alpha \boldsymbol{R})\boldsymbol{I} = \boldsymbol{E} \tag{3}$$

where

$$G_{nm} = \sum_{k=1}^{K} \omega\left(\vec{r}_k\right) c_n\left(\vec{r}_k\right) c_m\left(\vec{r}_k\right)$$

$$E_n = \sum_{k=1}^{K} \omega\left(\vec{r}_k\right) c_n\left(\vec{r}_k\right) B_Z^t\left(\vec{r}_k\right).$$

Noticing that $\omega\left(\vec{r}_k\right)$, $B_Z^t\left(\vec{r}_k\right)$ and α are input parameters, only the geometrical coefficients $c_n\left(\vec{r}_k\right)$ need to be calculated in order to invert Eq. (3) and solve for the optimal set of currents. Given the azimuthal symmetry of the problem, the set of target values can be defined on a plane to save computation time. Minimization of

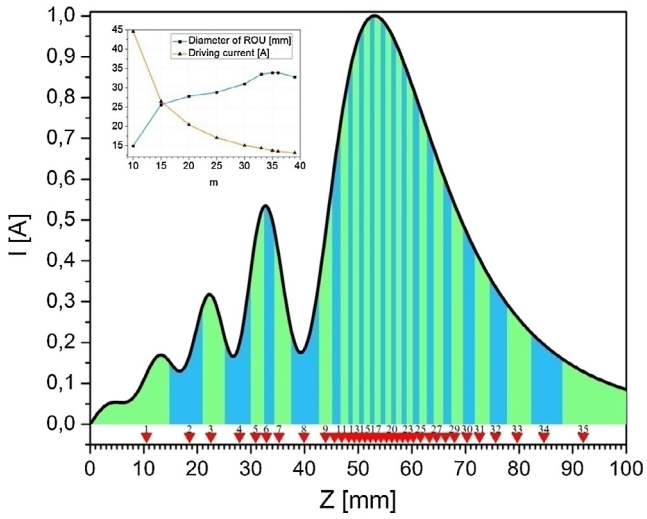

Fig. 1. Optimized current density obtained through the described algorithm. Only half of the density function is shown (impair function). Color bands represent equally integrated currents (see text). The triangles determine the positions for the discretized current paths corresponding to the single-current solution (35 conductors for half coil were chosen in this case). *Inset:* Dependence of the driving current (needed to generate 200 mT/m) and effective diameter for a uniform gradient volume (±2.5%) as a function of the number of loops.

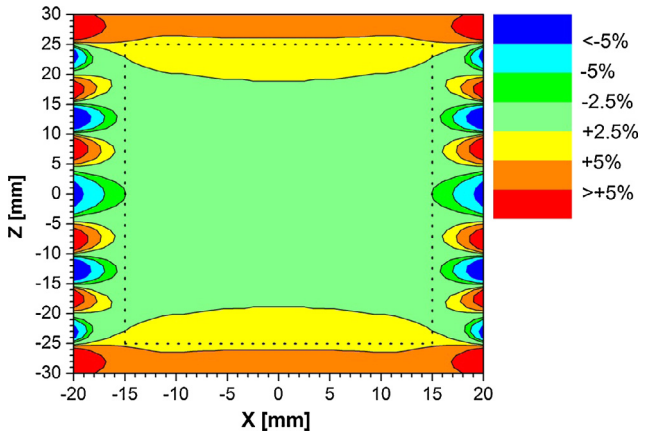

Fig. 2. Theoretical magnetic field gradient uniformity map corresponding to the discretized solution shown in Fig. 1. Observe that the uniformity within the specified region (dotted square) is within ±2.5%.

Φ comes from solving the $N \times N$ first order simultaneous equations obtained from forcing all $\partial\Phi/\partial I_n$ to zero. The result is a discrete current density which arises from the I_n currents values of the N conductors (Fig. 1).

3. Single current approach

After the current density was calculated, we have to face the problem of faithfully reproducing the function on the surface of a cylindrical former. This involves determining the current paths the conductor must follow to best approximate the optimized current density, with the additional constraint that the coil should be driven by a single current source. All these demands can be met by dividing the total current (integral of the current density) by m, the selected number of discrete conductors to locate on the surface of the former. The driving current will then be the total current divided by m. The current paths can be calculated by integrating the current density until the driving current is accumulated. The corresponding conductor must be placed inside the integration range at the position having equally integrated currents at both sides (Fig. 1).

Care must be taken in selecting the number of conductor loops m. A large value for m plays in favor for a higher field-to-power ratio, but also increases the inductance and resistance of the coil. However, it is also seen (inset in Fig. 1) that a minimum number of conductors is needed to accurately approximate the optimized current density. Thus, a situation of compromise is encountered. The purpose of the coil and current source specifications will determine the best design.

The Biot-Savart law was again used to write an algorithm in C++ for testing the final design. As shown in Fig. 1, the treated case uses 70 conductors to approximate the optimized current density. The test is carried out by placing loop conductors at the positions obtained from the optimization algorithm. All conductors are driven with the same current value. A first coil designed using this method was presented in a previous work, and the method was validated by measurements in a prototype [22]. Here we present an improved solution for a shorter coil (same VOI), were the weighting factor of the power term was slightly increased (see Eq. (2)). Fig. 2 shows the obtained field map corresponding to the current density of Fig. 1. For this coil the radial uniformity of the gradient is about 67.8%, it has an efficiency of 14.6 mT/m A, an electric resistance of ~880 mΩ and an inductance of ~124 μH. Coil dimensions are 50 mm diameter and 184 mm length.

4. Multiple-current approach

Single current solutions are very attractive for simplicity. However, in the context of field-cycling technology, multi-purpose coils rather open other possibilities for shimming the B_0 field, compensating field offsets and time-dependent corrections of thermal shifts. Active control of both the gradient and B_0 fields uniformities are favored by this approach, although one has to cope with an increasing hardware complexity. Multi-purpose coils can be handled by variable-geometry coils or, multi-winding coils feed by a set of independent power supplies. Variable-geometry designs include a higher mechanical complexity. In contrast, multiple-winding coils of fixed geometry are much simpler to build, at the cost of multiple powering.

The fact that the used algorithm starts off with discrete conductors, facilitates the analysis of coils based on independent localized windings. These designs have the great advantage that no conversion to a one-current solution is required, although driving these coils needs as many current sources as independent elements. It should be emphasized that only a few conducting elements can lead to gradient coil solutions with a better uniformity (±2.5%) volume to net coil volume ratio than single-current solutions. The design and prototype here presented proves this point.

The algorithm and computational procedure used for the optimization of this coil is the same as the employed for the single-current case. For a suitable comparison between the two coils, both designs were optimized having the same diameter of 50 mm. To keep the design as practical as possible one should try to minimize the number of elements N, since each added element demands an extra independent current source. Having this in mind, we searched for the smaller N that covers the targeted VOI following the next criterion: starting from a heavily power-dissipation oriented optimization (high α in Eq. (2)); successively more weight was put on the ROU (region of uniformity) optimization until it reached the targeted size (VOI). Then pass to the next N value. This procedure ensures finding the most power efficient design for each N value.

The final design consists of 18 equally spaced current elements distributed over a length of 90 mm. Opposed elements are con-

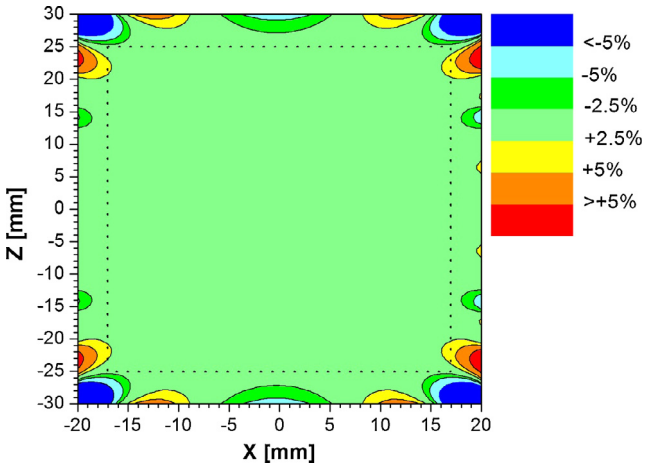

Fig. 3. Magnetic field gradient uniformity map for the simulated multiple-element coil. The figure shows the excellent performance in radial uniformity that can be reached within the active volume of this coil, for a proper current distribution.

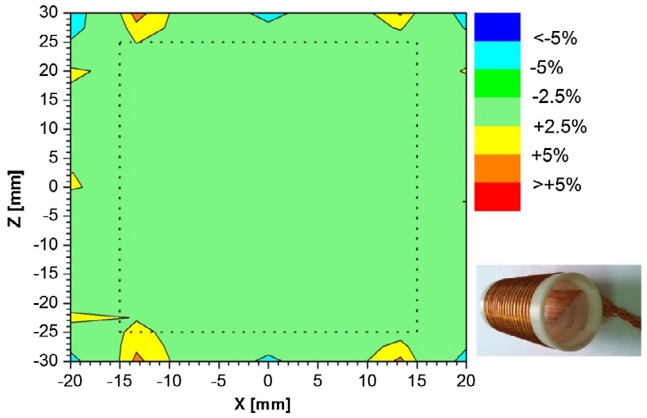

Fig. 4. Measured field map. The sample (dotted rectangle) is contained inside a volume of uniformity tolerance within ±2.5%.The inset shows the multiple-element prototype coil. The current paths that connect each anti-Helmholtz pair are shown to be in the inner side of the coil former.

nected to resemble 9 anti-Helmholtz pairs, with the same zero-field coordinate at the center of the coil. This configuration reduces the number of independent current sources needed to drive the coil. To our knowledge, the proposed arrangement of simultaneously powered combined anti-Helmholtz independent units has never been proposed nor tested before.

To enhance current efficiency and to avoid unpractical current values in the constructed prototype, 7 turns of 0.6 mm copper wire were used for each element. Questions arose as to how to place these seven turns of wire without degrading the calculated gradient uniformity. To solve this problem we simulated a few hand-picked configurations for the placement of the wires and compared the resulting uniformity maps. These configurations allowed the variation of the radial parameter in a 'layer per layer' fashion. The best configuration was found to be 4 turns in the first (inner) layer and 3 in the second (outer) layer (see the corresponding field-map in Fig. 3).

Although other configurations work just as well from a performance perspective, this one was chosen because of ease in construction. The implementation of multilayer gradient coil shows the advantage of improving the efficiency while keeping reasonable resistance values [28]. Since we do not change the wire diameter, the selected configuration yields:

$$\eta_7 = 7\eta_1; \quad R_7 = 7R_1; \quad L_7 \approx 2L_1$$

where the sub index 7 means configuration of seven turns in comparison with one, and η, R and L stands for efficiency, resistance and inductance respectively. This implies that even though the simultaneous switching [26] performance of the multiple-element coil degrades, the efficiency increases considerably.

A prototype was tested in order to validate the simulated results. The coil former was chosen to be of polyacetal resin (Delrin). This material offers good dimensional and thermal stability, while having optimal mechanical properties for its machining on a lathe. The machined former has inner and outer diameters of (47 ± 1) and (50 ± 1) mm respectively, and a total length of (120 ± 1) mm. Each independent element was constructed by winding AWG19 copper wire into milled grooves of (0.50 ± 0.05) mm in depth on the external former surface.

Magnetic field maps were obtained using a Lake Shore 475 DSP gaussmeter. The probe of the instrument was mounted on a home-made computer controlled rail with a position accuracy of (250 ± 2) μm. Measurements were taken at 7 longitudinal lines, each covering the range $[-27.5; 27.5]$ mm of the Z coordinate at different radial positions (in the same plane). The probe of the gaussmeter was guided by a wooden insert, which was milled to fit tightly inside the inner diameter of the former. Seven holes were also milled on this wooden piece to ensure radial positioning of the probe during measurements. The measured magnetic field map can be observed in Fig. 4.

The magnetic field was measured for the powered coil at 18 equidistant positions separated 2.5 mm each other (10 steps of the step-motor) along the Z-axis, covering a longitudinal range from (-20.00 ± 0.25) mm to (20.00 ± 0.25) mm (Fig. 5). The mag-

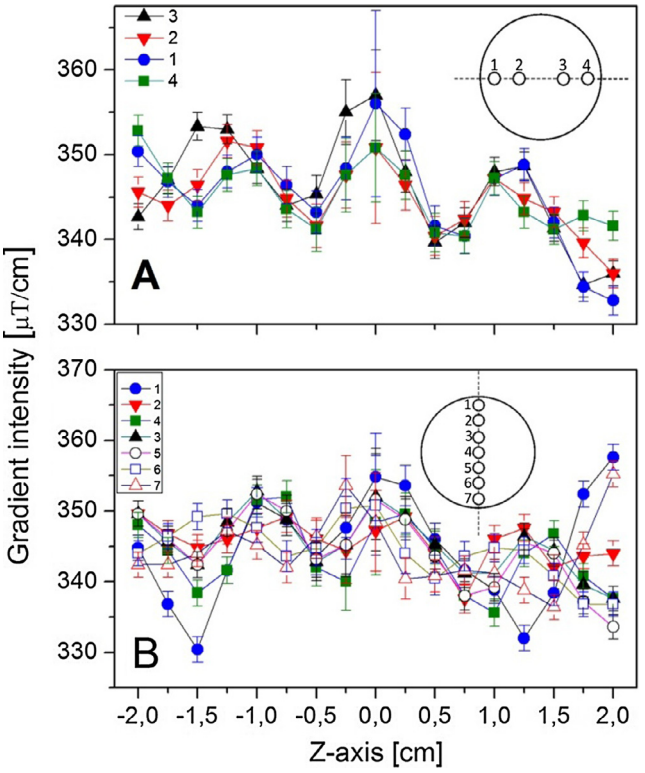

Fig. 5. Magnetic field gradient measured along the Z-axis of the multiple-element coil at different radial positions. (A) - Horizontal positions. (B) - Vertical positions. Observed fluctuations are within the ±5% of uniformity within the ROU. In figure A, positions 2 and 3 refer to (9.5 ± 0.5) mm and positions 1 and 4 to (15.8 ± 0.5) mm. In figure B: 4 is the center, 3 and 5 correspond to (6.3 ± 0.5) mm, 2 and 6 to (12.6 ± 0.5) mm while 1 and 7 to (18.9 ± 0.5) mm.

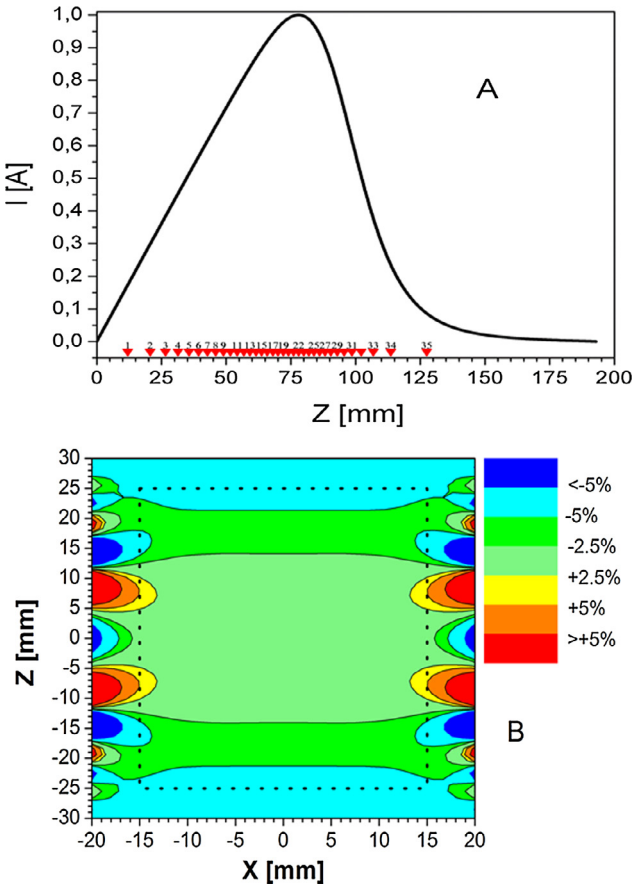

Fig. 6. Simulated coil using the target field approach. A: current density and discretization for a single-current assembly. B: field map. Observe that the uniformity within the VOI (dotted rectangle) does not comply with a ±2.5% tolerance.

netic field was measured five times at each position. The averaged values were used to derive the corresponding field gradient. Note the influence of the mechanical imprecision of the assembly and measurement set-up, causing variations between adjacent positions not only along the longitudinal axis but also in transversal direction. The remarkable point here is that all the values stay within 5% deviation, even those that are outside the ROU.

A remarkable feature can be observed in Figs. 3 and 4: reducing the length of the VOI to 40 mm, the radius of the uniformity volume can be extended to as much as 20 mm. This entails seizing 80% of the radial space occupied by the effective volume of the coil with a magnetic field gradient uniformity tolerance within the ±2.5%.

5. Discussion

The proposed method was previously tested in a single-current coil. The computed wiring and the simulated field map were examined in a home-made prototype [22]. Here we present a new optimization of the same coil, using the same algorithm, and showing an improved performance. We may compare this single-current coil with equivalent solutions obtained from different optimizations based on the well-known target field approach, as it is one of the most widely used and accepted methods for gradient coil design [8,29]. The guidelines for longitudinal gradient optimization described in Ref. [29] were followed in detail, for similar coil dimensions as used in our case. A function $f(Z) = 1/[1 + (Z/d)^{12}]$ was used to define the target field along the Z-axis (d stands for the length where the gradient is required to be uniform). The resulting half current density is shown in Fig. 6A, and the calculated field map is shown in Fig. 6B. In contrast with the calculated efficiency of 13.6 mT/m A [22] and 14.6 mT/m A (this work), the target field approach solution shown in Fig. 6 has a calculated efficiency of 8.3 mT/m A (for 70 conductors).

From the uniformity map it can be seen that the design does not perform to our demands. Nevertheless, it is noteworthy to mention that a discretization process with 45 conductors derives in a solution that tightly fits our sample, although the electric parameters of the coil are different.

A more valuable comparison to our case can be made by using the target field method including power dissipation into consideration, as originally described by Turner [1]. The method was implemented as described in [8], finding the Lagrange multipliers and using the inverse Fourier transform to obtain the current density. The resulting half current density is shown in Fig. 7A and the corresponding field map is shown in Fig. 7B.

The solution is obtained for a field defined as linear on the surface of a cylinder concentric with the coil, at $r = R/4$ and $z = (0.1).n.R_0$, where r is the radial coordinate, $n \in [1, 10]$ and R_0 is the coil radius. The method was implemented using the same coil and gradient uniformity parameters as needed by our application. The solution was also calculated by distributing the target field points along the axis of the coil, with minor differences in the results. For both cases the calculated efficiency of the resulting solution is ~13.7 mT/m A. From these results it turns clear that the inclusion

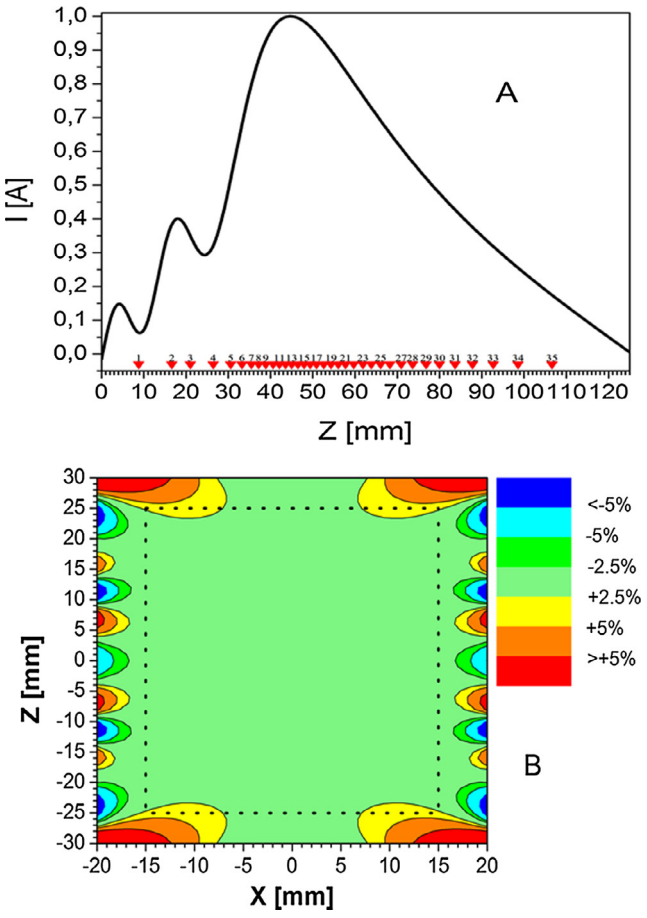

Fig. 7. Simulated coil using the target field approach with power minimization. A: current density and discretization for a single-current solution. B: gradient uniformity map. Observe the improvement of the uniformity within the VOI (dotted rectangle) if compared with Fig. 6B.

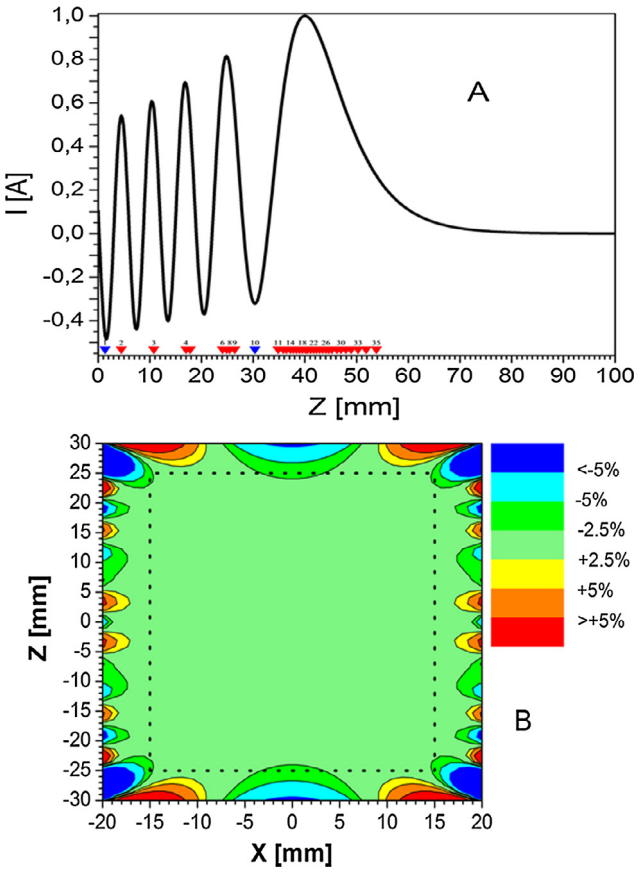

Fig. 8. Simulated coil using the target field approach with inductance minimization. A: current density and discretization for a single-current assembly. B: uniformity map. Observe the reduced length for the obtained coil (108 mm) and the tendency to superpose the position of the conductors. Also observe the negative currents that are intercalated in the solution when the position for a conductor coincides with an extreme in the negative density (blue triangles).

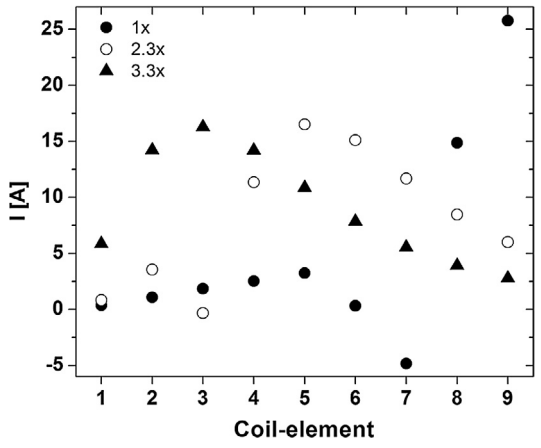

Fig. 9. The multiple-current approach allows setting different current distributions for the coil-elements. In this way, the same coil may produce different magnetic field maps: in the figure, each current distribution corresponds to a different ROU. Filled circles correspond to the case where the ROU fits the VOI (gradient efficiency 1×). Open circles correspond to a 2.2× gradient efficiency and triangles to a 3.3× gradient efficiency. Compare with Table 1 and Fig. 10.

of power optimization improves the coil performance (compare Figs. 6B and 7B). We may also compare Fig. 7B (target field with power optimization) with Fig. 2 (matrix inversion with power optimization), and the result previously obtained in [22]. We can see

Table 1
Calculated ROU and efficiency for different current distributions in a multiple-element coil. See Figs. 9 and 10.

	Red	Green	Black
ROU (mm^2)	38 × 40	38 × 12	11 × 9
Power (W)	206.6	202.7	210.7
Efficiency (mT/A m)	6.86	15.75	22.89
Relative efficiency	1	2.3	3.3

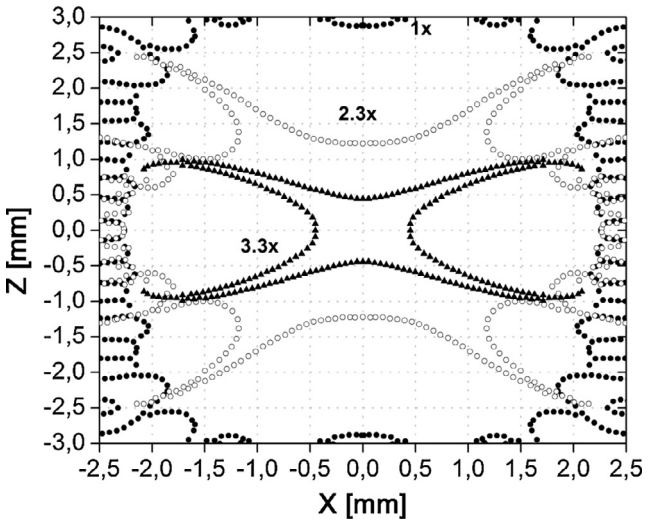

Fig. 10. Three different ROU produced with the same coil. The smaller the ROU, the larger the coil efficiency: filled circles correspond to the case where the ROU fits the VOI (1× efficiency); open circles stands for a 2.2× efficiency and triangles for a 3.3× efficiency. These maps correspond to the current distributions shown in Fig. 9.

that these results are equivalent within a non-uniformity of ±2.5%, that is, they do not show a critic dependency on the employed mathematical algorithm.

Finally, we compare with the minimum inductance target field optimization [8]. Specifying the field as linear on the axis of the coil the method gives a poor radial uniformity, as already observed by other authors [30]. An exhaustive analysis of the involved parameters was carried out to ensure an optimal solution (within the dimensions and restrictions of our case). The current density shown in Fig. 8A arises from a field defined as linear at $r = R/4$ and $z = (0.075).R_0.n$, with $n \in [1, 12]$. The corresponding uniformity map can be observed in Fig. 8B. Due to the minimum inductance condition, the method tend to pack the conductors into a small length (see Fig. 8A), resulting in an increase of the theoretical efficiency (17.8 mT/m A). Such solutions holds a drawback, since the tightly packed conductors in the largest lobe of the current density are scarcely separated, thus being a limitation for the practical implementation (conductors may be superposed but this may introduce important errors if not properly positioned according to the calculated discretization). The oscillatory character of the optimized current density is also problematic at the discretization stage, particularly for coils of reduced dimensions like we consider in this work. Errors occur when the current density crosses zero, where integrated currents which determine conductor's positions cancel themselves out. Moreover, no conductors will be placed by the algorithm in lobes with area smaller than the integrated current. This imposes a restriction to the number of conductors into which the current density can be partitioned.

Now we confront the radial uniformity and the coil efficiency with the multiple-current equivalent. The obtained results show the excellent performance that can be obtained with this coil

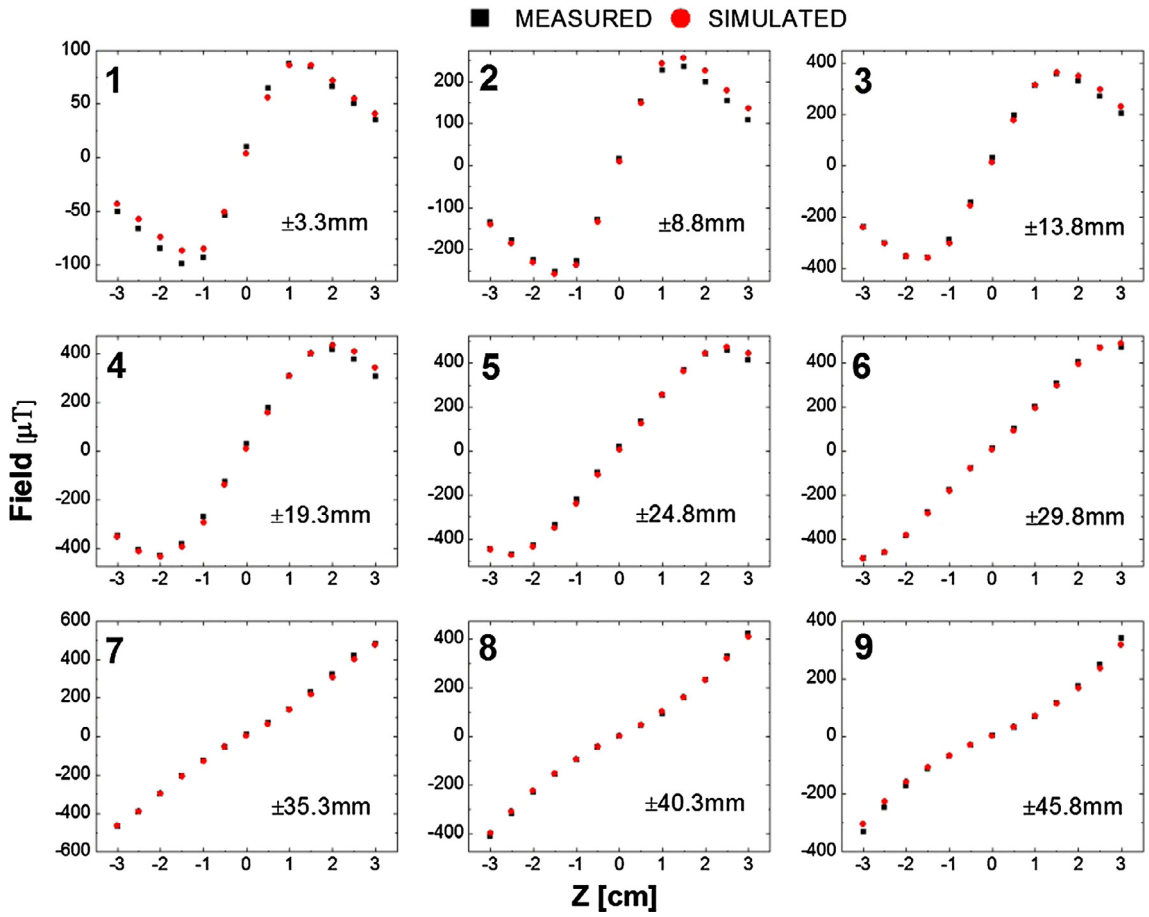

Fig. 11. Magnetic field along the *Z*-axis measured and simulated for each anti-Helmhotlz pair element. Element 1 corresponds to the inner pair, while element 9 corresponds to the external pair. The inset in the figures indicates the position along the *Z*-axis in mm of each pair.

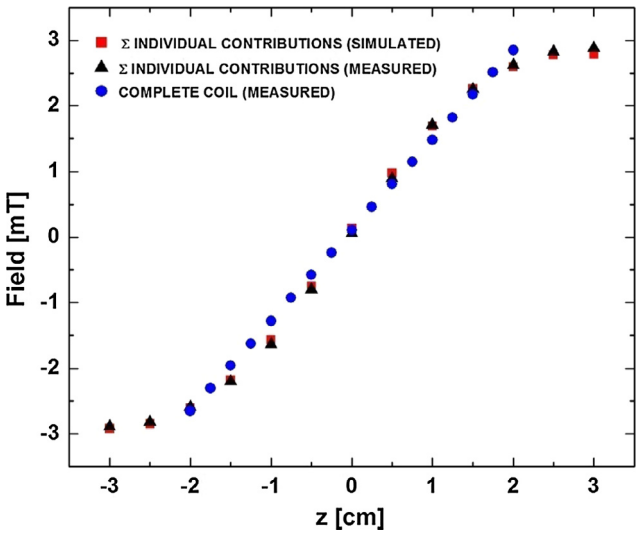

Fig. 12. Magnetic field along the z-axis for the multiple-element coil. Red (squares) and black (triangles) points correspond to the sum of the measured and simulated individual contributions, while the blue points (circles) correspond to the measured field with all elements simultaneously powered. Experimental errors are contained within the symbol size. (For interpretation of the references to color in this figure legend, the reader is referred to the web version of this article.)

(see Fig. 3). An interesting advantage of the multiple-element approach relays in the possibility to adjust the current of the anti-Helmholtz pairs according to the required specifications. For example, it is possible to gain efficiency by reducing the region of uniformity (ROU), thus increasing the gradient magnitude at the same power (see Fig. 9 and Table 1). The figure shows the increase from 6.86 mT/A m (1×) to 15.75 mT/A m (2.3×) and even 22.89 mT/A m (3.3×) gradient efficiency at the same power consumption, at the cost of a reduced ROU.

These results suggest that the same coil can be configured to be more efficient for a similar power, at the cost of a reduction in the ROU. The field maps corresponding to the current distributions shown in Fig. 9 can be observed in Fig. 10. Here we can see the noticeable sensitivity of the coil for different current distributions, even when the net dissipated power is nearly the same for all the cases.

Fig. 11 show the simulated and measured magnetic field along the Z-axis of the multiple-element coil for each anti-Helmholtz pair, each powered with the corresponding current (see Fig. 9 for 1×). The sum of these contributions builds-up the final gradient, as can be observed in Fig. 12. These figures suggest the great flexibility of the design for a uniform gradient after a proper current setting of the individual elements.

The switching behavior of the coil was analyzed using the mathematical model described in reference [26]. Self and mutual inductances were measured in the prototype, see Table 2 (self inductances are measured with all the remaining elements open, while the net inductance is measured with all the remaining elements in shortcut). It was found that only the three closest neighbors contribute to the mutual inductance, for each element. The simulated response of the system is based on the measured cross coupling inductive matrix. Fig. 13 shows the response of the sys-

Table 2
Lo: 7-turns element's self-inductance. *L*: element's inductance in presence of coupling with all other elements. *R*: resistance of each element. Note that the inductive couplings are weak since the net inductance after mutual couplings do not differ too much from the self-inductance values. This will be reflected in favorable time-dependent effects.

Element	*Lo* ± 2 (μH)	*L* ± 2 (μH)	*R* ± 2 (mΩ)	*I* ± 0.01 (A)
1	115	126	217	3.68
2	123	140	235	2.12
3	126	145	235	−0.69
4	121	142	231	0.90
5	113	132	226	0.46
6	115	129	223	0.36
7	125	137	225	0.26
8	135	142	223	0.15
9	183	188	226	0.05

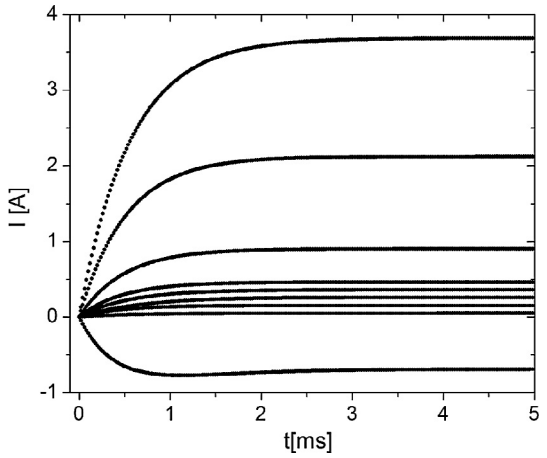

Fig. 13. Turn-on behavior of the coil when the largest ROU set-up is used. Note that the setting-times of all the coils are nearly coincident. From top to bottom the coil-element number is 1–2–4–5–6–7–8–9–3.

tem for the simultaneous switching of the elements using idealized independent power supplies. The highest voltage needed in this example is less than 1 V. After the transient time (about 3 ms for the largest ROU in the simulated conditions) and once the currents values are stable, the generated gradient corresponds to the passive solution (200 mT/m @ ∼5 W). The switching time can be optimized by a proper powering network and an adequate control strategy, thus enabling preenphasis or other particular switching conditions. Since the sampling of a single current for the control loop is not possible in this case, a direct sensing of the generated field must be considered. Details of this sort are however outside the present scope. Fig. 13 shows that, against the mutual inductance coupling between the elements, it is possible to switch a gradient coil based on the multiple-current approach.

6. Conclusions

A computational cost-effective, simple and intuitive optimization method for designing longitudinal gradient coils was discussed. The method was successfully used for the design of fast field-cycling magnets in the past. Simulated results were experimentally validated in real prototypes. The matrix inversion formalism with power optimization here presented is compared with different versions of the target field approach. When power minimization is considered, both methods perform equivalently. A contrast however exists in the difficulty of implementation. The proposed approach shows the advantage of a straightforward way, easy to learn and write down. The results of this comparison suggest that the key-feature of the optimization process does not rely on the mathematical machinery itself, but on the selected physical parameter used in the process. It is worth to mention that although the target field approach with power optimization was mentioned long ago in reference [1], this is the first time a uniformity map obtained with this methodology is shown and, simultaneously compared to its matrix inversion equivalent and the target field minimum inductance method.

We presented an original multiple-element configuration based on 9 anti-Helmholtz pairs showing an excellent radial uniformity. Such coil seizes 80% of the radial length it occupies with a nonuniformity of less than ±2.5%, and over a length that represents 44% of its total axial extension. Multiple-element solutions are very much attractive in FFC technology since they can be used to fulfill different tasks during the evolution of an experiment: it can be used to generate intense gradients, and actively correct for the magnetic field inhomogeneities of the FFC B_0 magnet during signal acquisition [31].

Pulsed gradients based on the multiple-current approach demands for particular powering and control solutions that are outside the scope of the present. However, we may anticipate that a multiple channel power supply with a feedback based on the direct sampling of the field, plus iterative learning control and statistical signal characterization (or feedforward strategies) may be of potential success.

Both solutions here presented fits very well with the requirements for a compact gradient unit to be located inside our FFC magnet. Field-cycled images using the coils here described will be shown soon elsewhere.

Acknowledgments

This work was supported by funds from FONCyT – Argentina (PICT-2013-1380), Ministerio de Ciencia y Tecnología (Provincia de Córdoba – Argentina) and Secretaría de Ciencia y Tecnología – Universidad Nacional de Córdoba, Argentina. The Authors acknowledge the collaboration of M. Eisenreich (TU-Imenau, Germany) and W. Zaninetti in the set-up of the computerized positioning machine.

References

[1] R. Turner, Gradient coil design: a review of methods, Magn. Reson. Imag. 11 (1993) 903–920.
[2] J. Jin, Electromagnetic Analysis and Design in Magnetic Resonance Imaging, CRC Press, Boca Ratón, 1999.
[3] F. Noack, NMR field-cycling spectroscopy: principles and applications, Prog. Nucl. Magn. Reson. Spectrosc. 18 (1986) 171–276.
[4] E. Anoardo, G. Galli, G. Ferrante, Fast-field-cycling NMR: applications and instrumentation, Appl. Magn. Reson. 20 (2001) 365–404.
[5] R. Kimmich, E. Anoardo, Field-cycling NMR relaxometry, Prog. Nucl. Magn. Reson. Spectrosc. 44 (2004) 257–320.
[6] F. Fujara, D. Kruk, A. Privalov, Solid state field-cycling NMR relaxometry: instrumental improvements and new applications, Prog. Nucl. Magn. Reson. Spectrosc. 82 (2014) 39–69.
[7] R. Turner, R.M. Bowley, Passive screening of switched magnetic field gradients, J. Phys. E: Sci. Instrum. 19 (1986) 876–879.
[8] R. Turner, Minimum inductance coils, J. Phys. E: Sci. Instrum. 21 (1988) 948–951.

[9] R.C. Compton, Gradient Coil Apparatus for a Magnetic Resonance Systems, U.S. Patent 4.456.881, January 18th 1982.
[10] S. Crozier, D.M. Doddrell, Gradient-coil design by simulated annealing, J. Magn. Reson. A 103 (1993) 354–357.
[11] K.H. Schweikert, R. Krieg, F. Noack, A high-field air-cored magnet coil design for fast-field-cycling NMR, J. Magn. Reson. 78 (1988) 77–96.
[12] E. Wong, A. Jesmanowicz, J.S. Hyde, Coil optimization for MRI by conjugate gradient descent, Magn. Reson. Med. 21 (1991) 39–48.
[13] J.F. Schneck, M.A. Hussein, W.A. Edelstein, Transverse Gradient Field Coils for Nuclear Magnetic Resonance Imaging, U.S. patent 4.646.024, November 2nd, 1983.
[14] W.A. Edelstein, J.F. Schneck, Current Streamline Method for Coil Construction, U.S. patent 4.840.700, July 13th, 1987.
[15] R.J. Sutherland, Selective Excitation in NMR and Considerations For Its Use in Three Dimensional Imaging (Ph.D. Thesis), University of Aberdeen, Aberdeen, 1980.
[16] P.T. While, L.K. Forbes, S. Crozier, Designing gradient coils with reduced hot spot temperatures, J. Magn. Reson. 203 (2010) 91–99.
[17] A. Trakic, F. Liu, H. Sanchez Lopez, H. Wang, S. Crozier, Longitudinal gradient coil optimization in the presence of transient eddy currents, Magn. Reson. Med. 57 (2007) 1119–1130.
[18] D.C. Alsop, T.J. Connick, Optimization of torque-balanced asymmetric head gradient coils, Magn. Reson. Med. 35 (1996) 875–886.
[19] P. Mansfield, B.L.W. Chapman, R. Bowtell, P. Glover, R. Coxon, P.R. Harvey, Active acoustic screening: reduction of noise in gradient coils by Lorentz force balancing, Magn. Reson. Med. 33 (1995) 276–281.
[20] S. Kruber, G.D. Farrher, E. Anoardo, Air core notch-coil magnet with variable geometry for fast-field-cycling NMR, J. Magn. Reson. 259 (2015) 216–224.
[21] R. Turner, Gradient coil systems, in: D.M. Grant, R.K. Harris (Eds.), Encyclopedia of Nuclear Magnetic Resonance, vol. 4, Wiley, New York, 1996.
[22] G.A. Dominguez, J.A. Romero, E. Anoardo, Longitudinal gradient-coil with improved uniformity within the volume of interest, in: IEEE Biennial Congress of Argentina (ARGENCON), Bariloche, 2014.
[23] M. Westphal, H. Schmidt, Electric Arrangement for Operation of a Gradient Coil with Several Power Supplies, U.S. patent 6.479.997, November 12th, 2002.
[24] W. Arz, M. Gebhardt, F. Schmitt, Switchable Longitudinal Gradient Coil, U.S. patent 6.515.479, February 4th, 2003.
[25] Q. Liu, Gradient Coil Set Capable of Producing a Variable Field of View, U.S. patent 6.630.829, October 7th, 2003.
[26] S. Kruber, G. Farrher, E. Anoardo, New Magnet Design for Fast-Field-Cycling Nuclear Magnetic Resonance, IEEE Lat. Am. Trans. 11 (2013) 251–256.
[27] R.A. Lemdiasov, R. Ludwig, A stream function method for gradient coil design, Conc. Magn. Reson. B 26 (2005) 67–80.
[28] R. Bowtell, P. Robyr, Multilayer gradient coil design, J. Magn. Reson. 131 (1998) 286–294.
[29] R. Turner, A target field approach to optimal coil design, J. Phys. D: Appl. Phys. 19 (1986) L147–L151.
[30] Q. Liu, *A shielded transverse gradient coil for in-vivo NMR* (M.Sc. Thesis), second ed., University of Alberta, Edmonton, 1991.
[31] H.H. Segnorile, G.O. Forte, G.D. Farrher, E. Anoardo, NMR-SSC magnetic field profiler applied to magnetic field shimming, IEEE Lat. Am. Trans. 11 (2013) 257–262.